Nanoscale

PAPER

View Article Online
View Journal | View Issue

Cite this: *Nanoscale*, 2023, **15**, 2767

Eco-friendly screen printing of silver nanowires for flexible and stretchable electronics†

Darpan Shukla, Yuxuan Liu and Yong Zhu*

Screen printing is a promising route towards high throughput printed electronics. Currently, the preparation of nanomaterial based conductive inks involves complex formulations with often toxic surfactants in the ink's composition, making them unsuitable as an eco-friendly printing technology. This work reports the development of a silver nanowire (AgNW) ink with a relatively low conductive particle loading of 7 wt%. The AgNW ink involves simple formulation and comprises a biodegradable binder and a green solvent with no toxic surfactants in the ink formulation, making it an eco-friendly printing process. The formulated ink is suitable for printing on a diverse range of substrates such as polydimethylsiloxane (PDMS), polyethylene terephthalate (PET), polyimide (PI) tape, glass, and textiles. By tailoring the rheological behaviour of the ink and developing a one-step post-printing process, a minimum feature size of 50 μm and conductivity as high as 6.70×10^6 S m^{-1} was achieved. Use of a lower annealing temperature of 150 °C makes the process suitable for plastic substrates. A flexible textile heater and a wearable hydration sensor were fabricated using the reported AgNW ink to demonstrate its potential for wearable electronic applications.

Received 21st October 2022,
Accepted 19th December 2022

DOI: 10.1039/d2nr05840e

rsc.li/nanoscale

Introduction

Printed electronics (PE) is revolutionizing the field of flexible and stretchable electronics.[1] Features like low-cost fabrication, less material wastage, adaptability to a roll-to-roll manufacturing process, and compatibility with elastomeric substrates have attracted researchers to develop sensors for non-planar-surfaces like human skin.[2]

A wide variety of printing methods, broadly defined as non-contact and contact-based, have beenreported for printing nanomaterial-based inks on stretchable and flexible substrates.[3] Among different non-contact printing methods, electrohydrodynamic (EHD) printing offers high resolution printing by producing droplets much smaller than the nozzle diameter. This unique feature provides printability of metal nanowires (NWs) (generally >10 μm in length) without the issue of nozzle clogging as encountered in inkjet printing.[4–6] However, EHD printing suffers from low throughput which hinders its applicability at the commercial level.[7] Gravure printing, on the other hand, is a contact-based printing method and is suitable for large-scale applications due to its low cost, high speed, and compatibility with roll-to-roll processes.[8] However, the issue of ink drag-out from the cells during doctor blade wiping can lead to deteriorated pattern fidelity.[9]

Screen printing involves deposition of ink by pressing it through a patterned stencil with a squeegee.[10] It is well suited for rapid and scalable manufacturing of printed electronics due to its low-cost and facile operability.[11,12] A distinctive feature of screen printing is that it offers printing of high-aspect-ratio patterns.[13] Typically, a screen-printing process is limited to a resolution of 50–150 μm in accordance with a screen mask resolution of 40–120 μm.[10] However, higher-resolution patterns can be achieved by modifying the surface energy of the substrate and/or viscosity of the printing ink.[14–17]

Recently, nanomaterials such as metal nanoparticles (NPs), metal nanowires (NWs), carbon nanotubes (CNTs), graphene, and conductive polymers have been used for formulating conductive inks for screen printing.[12] Among these nanomaterials silver NWs (AgNWs) have received considerable attention for flexible and stretchable electronics due to their high electrical conductivity, mechanical robustness, and optical transparency.[18,19] For instance, Li *et al.* screen printed ultra-long AgNWs for fabricating flexible transparent conductive films and wearable energy storage devices. The high conductivity of 8.32×10^5 S m^{-1} and optical transparency (~80%) of the printed patterns made them a compelling replacement for the rigid indium titanium oxide.[14] Liang *et al.* formulated a water-based AgNW ink for fabricating stretchable conductors and wearable thin-film transistors on flexible substrates. A

Department of Mechanical and Aerospace Engineering, North Carolina State University, Raleigh, NC 27695, USA. E-mail: yzhu7@ncsu.edu

†Electronic supplementary information (ESI) available: Fig. S1–S8. See DOI: https://doi.org/10.1039/d2nr05840e

minimum feature size of 50 μm and a high conductivity of 4.67×10^6 S m^{-1} were achieved.[19] Furthermore, a thixotropic ternary ink consisting of hydrous ruthenium oxide ($RuO_2{\cdot}xH_2O$) NPs, AgNWs, and graphene oxide was used to screen print micro-supercapacitors. The hybrid ink aided in achieving a high resolution of 50 μm and conductivity of 5×10^5 S m^{-1}.[20] Despite the great success in formulating AgNW-based screen-printing inks for flexible and stretchable electronics, a few challenges remain: (1) the existing inks typically involve complex formulations. (2) The inks are not eco-friendly (*e.g.*, the polymer binder is not biodegradable). (3) High conductive particle loading, and multiple post-printing steps are typically required to achieve the desired electrical conductivity. In addition, developing a single printing process, which is suitable for printing on various flexible substrates like plastics, elastomers, papers, and rough textile surfaces, is also desirable.[21–23]

Water-based screen-printing inks have aroused interest due to their eco-friendly nature as they address the disposability threat possessed by organic solvents.[24] Camargo *et al.* screen-printed disposable electrodes by formulating an eco-friendly water-based conductive ink comprising of chitosan, graphite powder, and glycerol.[24] Similarly, Franco *et al.* formulated a graphene ink by using carboxy methyl cellulose as a water-soluble polymer.[25]

In this work, we report the development of a AgNW based ink that comprises poly(ethylene) oxide (PEO) as a biodegradable binder and deionized (DI) water as a "green solvent" with no toxic surfactants in the ink formulation, making it an eco-friendly printing technology. A relatively low AgNW loading (7 wt%) and a single step low-temperature post-printing treatment feature the merits of low-cost screen printing. The screen printed AgNW lines exhibit conductivity as high as 6.70×10^6 S m^{-1}. Uniform and continuous lines with a minimum feature size of 50 μm are achieved by tailoring the rheological properties of the ink. In addition, it is capable of printing on diverse range of substrates such as polydimethylsiloxane (PDMS), polyethylene terephthalate (PET), polyimide (PI) tape, glass, and even rough textile surface, which is difficult to print with other printing methods. Lastly, wearable devices based on the printed AgNWs are demonstrated by fabricating flexible heaters on textiles and wearable hydration sensors on PDMS.

Results and discussion

Conductive inks for screen printing are usually a mixture of three components: conductive nano or micro particles as fillers, an organic binder/additive, and a solvent. Printability of the ink and conductivity of the printed patterns are influenced by solid loading, particle dispersion, and density of the conductive fillers.[19] Organic binders/additives in combination with solvents promote dispersion stability, particle wettability, and adhesion to the substrate.[8] They also provide the desired rheological behaviour to the ink for screen printing and regulating ink drying during and after printing.[26] In this work, AgNWs were used as conductive fillers for the ink. To tune the viscosity of the ink, poly(ethylene oxide) (PEO), a non-ionic water-soluble polymer, was used as a rheological agent. The high molecular weight of PEO (average $M_v \sim 1\,000\,000$) assists in dramatically increasing the viscosity of the ink and provided a shear-thinning thixotropic behaviour. Furthermore, it can act as a surfactant as the hydroxy groups in PEO can bond with the surface of AgNWs and improve their dispersion in the ink.[8] DI water and ethanol served as solvents for the ink. The key properties of non-toxic ethanol, *i.e.*, lower boiling point and lower surface tension than water, prevent undesirable aggregation of AgNWs, which results from contact line recession and dewetting during the evaporation process. However, the solubility of high molecular weight PEO in pure ethanol at room temperature is a challenge.[27] Therefore, a solvent mixture consisting of DI water and ethanol in the weight ratio of 50 : 50 was used. DI water was selected as the second solvent due to its environmental friendliness. In a typical ink formulation, PEO powders with four different concentrations (4%, 5%, 6%, and 7% weight ratio) were first mixed with ethanol and DI water by stirring for 24 h to form a homogeneous solution. Then, AgNWs were added into the PEO solutions to make four different inks with 7 wt% AgNW solid loading (Fig. 1a) and PEO weight ratio of 4% (AgNW Ink A), 5% (AgNW Ink B), 6% (AgNW Ink C) and 7% (AgNW Ink D). The inks were mixed for 30 min to obtain an even dispersion.

Performance of a screen-printed pattern is governed by the viscosity and rheological behaviour of the ink.[19] Therefore, rheological characterization of the ink was performed using a parallel-plate rheometer. Firstly, AgNW Ink B (7 wt% AgNWs with 5 wt% PEO) was tested alongside 5 wt% PEO solution (without AgNWs) to determine the influence of AgNWs on the rheological properties of the ink (Fig. S1a†). At the same shear rate of 0.1 s^{-1}, the viscosity of AgNW Ink B and 5 wt% PEO solution (without AgNWs) was 144.45 and 36.30 Pa s, respectively. The difference in viscosity was observed because NWs can act as active crosslinkers and can constitute a solid 3D network in the ink suspension causing higher viscosity.[19,20] Moreover, at low shear rates, random orientation of the AgNWs in the suspension causes an increase in viscosity. Hemmati *et al.* also observed that rheological behaviour and flow characteristics of the AgNWs depends on their solid content in the suspension[28] which in our work was fixed as 7 wt% among all PEO solutions. Furthermore, in the absence of a rheological modifier, the shear-thinning behaviour shown by the pure AgNW suspension is unsuitable for screen printing (viscosity of <1 Pa s) due to the formation of macroscopic AgNW aggregates above the 5 s^{-1} shear rate.[29] Based on the above-mentioned reasons, further rheological characterization was performed only on different wt% PEO solutions.

Fig. S1b† demonstrates that all PEO solutions (4%, 5%, 6%, and 7% weight ratio) exhibited shear thinning behaviour of a non-Newtonian fluid that can be observed through decreasing viscosity with an increasing shear rate. This characteristic

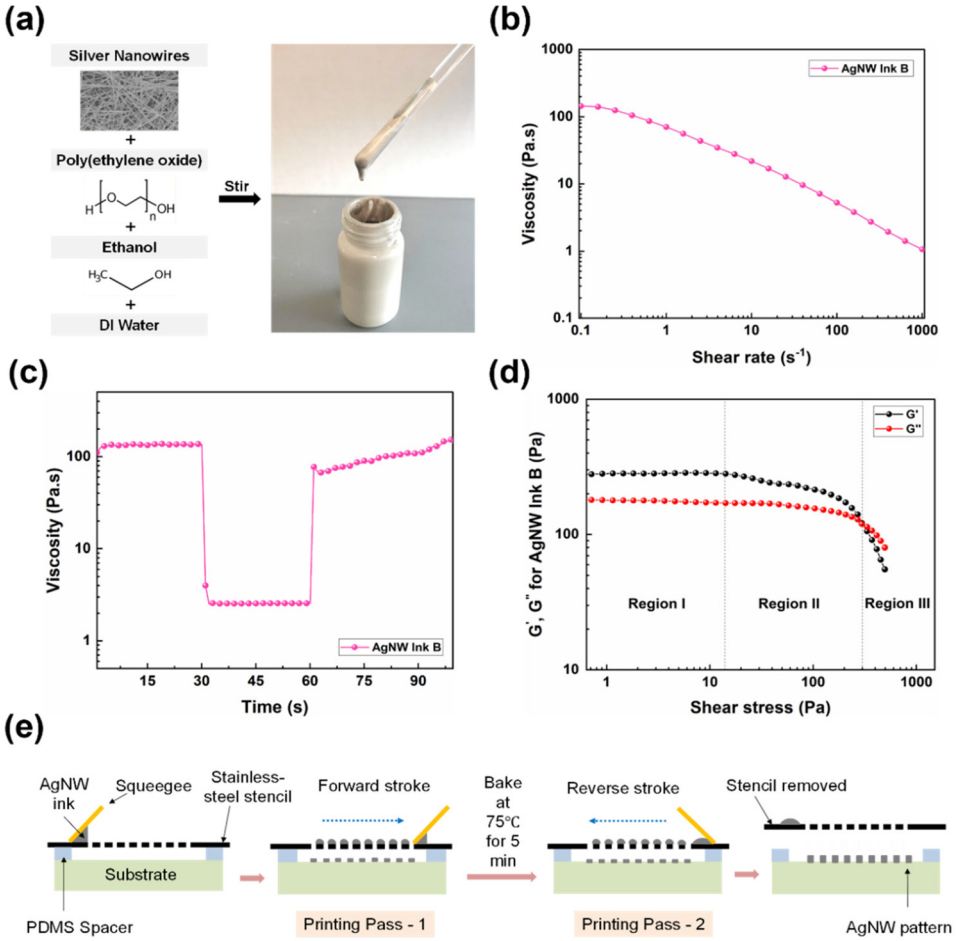

Fig. 1 (a) Constituents of AgNW based screen printing ink and photograph of AgNW Ink B (7 wt% AgNW–5 wt% PEO). (b) Viscosity as a function of the shear rate for AgNW Ink B. (c) Rheological behaviour of AgNW Ink B during the screen-printing process. (d) Oscillatory rheological test for AgNW Ink B showing variation of G' and G'' as a function of shear stress. (e) Illustration of the screen-printing process.

property allows for a high-resolution print as the ink rapidly recovers to its initial viscosity once the squeegee stroke has ended.[29] It can be observed that solutions with a higher PEO amount showed higher viscosity at the same shear rate. The degree of entanglements of the polymer coils increases with the polymer concentration, producing higher viscosity.[30]

Next, the screen-printing process can be categorized into three distinct steps in which each step is associated with a shear rate during the printing process. The first step involves ink transfer onto the stencil. In this stage, the ink is subjected to small deformations and low shear. During the second step (printing stroke), a large shear rate acts on the ink which makes it flow through the stencil/mesh screen.[29] In the final step, the ink progressively returns to the viscosity in the first step. The peak hold step test was conducted to simulate the above-mentioned steps in the printing process.[19,30,31] The test involved holding the PEO solution at different shear rates in three intervals as shown in Fig. S1c.† In the first interval, a shear rate 0.1 s^{-1} was maintained for 30 s. The second interval simulated the printing stroke with a shear rate of 200 s^{-1} for 30 s. Finally, the shear rate in the third interval was decreased to 0.1 s^{-1} and maintained for 200 s to observe the viscosity recovery after printing. 4 wt% PEO solution showed the lowest viscosity of 8.08 Pa s at the 0.1 s^{-1} shear rate at the time of 20 s. The solution recovered to 100% (at 90 s) of its initial viscosity after the shear rate was reduced from 200 to 0.1 s^{-1}. Although 4 wt% PEO solution displayed 100% recovery, its low viscosity could cause ink spreading after printing which could negatively impact the line resolution. Table S1† depicts that with increasing PEO concentration, the solution takes a longer time to recover to its initial viscosity. The imposed shear deformation during printing disrupts the entangled polymer coils. The longer recovery time of the solution with the higher PEO content is because the rate of disruption of the entangled polymer coils is higher than the rate of formation of the new ones.[32] Recovery time of the ink plays a crucial role in levelling the ink after printing, leading to a uniform deposition with no voids and/or irregularities.[17,27] Amongst all four PEO solutions, the one with 5 wt% PEO demonstrated the ideal rheological behaviour for screen printing. Henceforth, AgNW Ink B (7 wt% AgNWs with 5 wt% PEO) was tested in future experiments.

Fig. 1b demonstrates the viscosity at different shear rates from the steady-state flow step test. AgNW Ink B exhibited a shear thinning behaviour with a viscosity of 144.45 Pa s at 0.1 s^{-1} shear rate. The peak hold test in Fig. 1c and Table 1 show that AgNW Ink B recovered to 83.8% of the initial viscosity in 30 s after the printing stroke, which portrays the desirable elasticity of the ink. Usually, inks incorporating Ag particles/flakes can barely exceed 70% recovery.[26] The better performance of AgNW Ink B compared to particle-based inks stems from the outstanding properties of the AgNWs in the ink formulation. However, the recovery of AgNW Ink B was lower than that of the 5 wt% PEO solution. This was because of the combined influence of the rearrangement of polymer coils in PEO and reorientation of AgNWs from an aligned state at a high shear rate to a random network under a low shear rate.[28,32] Fig. S2 and Table S2† provide the recovery values for different wt% PEO solutions and AgNW-based inks. For AgNWs, the rate of rearrangement and hence, viscosity recovery is controlled by the wire–wire interaction and hydrodynamic forces, both of which depend on the AgNW content in the suspension.[28]

Oscillatory rheological measurements were conducted for AgNW Ink B to further characterize its viscoelastic effect in a stress sweep step test. Fig. 1d presents the variation of storage modulus G' (elastic component) and loss modulus G'' (viscous component) as a function of shear stress. The viscoelastic behaviour can then be evaluated using the loss factor $\tan(\delta)$ according to eqn (1)

$$\tan(\delta) = \frac{G''}{G'} \quad (1)$$

from eqn (1), it can be inferred that when $\tan(\delta)$ is higher than 1, the viscous component G'' will dominate and the ink will exhibit liquid-like behaviour. However, when $\tan(\delta)$ is lower than 1, the ink will demonstrate solid-like behaviour. Region I in Fig. 1d shows the linear viscoelastic region. Here, the ink can endure mechanical deformations without disrupting its molecular structure. With increasing shear stress, the ink structure starts to disintegrate and the value of G' and G'' gradually decreases, although AgNW Ink B still maintains elastic behaviour. At a shear stress of 306.9 Pa, the storage modulus becomes equal to the loss modulus ($G' = G''$). With further increase in the shear stress, G'' exceeds G' and the ink displays fluid-like behaviour.

Fig. 1e illustrates the screen-printing process. A laser cut stainless-steel stencil of ~100 μm in thickness was used. A thinner stencil can impart the mechanical flexibility needed to deform the stencil during the printing stroke.[10] An off-contact distance of 2 mm was used between the stencil and the substrate, achieved by using PDMS spacers whose adhesive surface provided the benefit of securing the stencil and the substrate during the printing process. The off-contact distance assists in applying the desired squeegee pressure to deform the stencil. It also prevents the stencil from resting back on to the wet printed layer, thus eliminating smudging of the printed pattern. During the printing stroke, the stencil bends and forms a contact between the stencil and the substrate. The ink fills into the stencil openings in front of the squeegee and finally, the stencil snaps back to its initial position transferring the ink on to the target substrate.[17] Traces from the first printing pass were baked for 5 min at 75 °C without removing the stencil. Baking is necessary because wet ink in the second printing pass cannot be overprinted without smearing and smudging. A second printing pass was performed by moving the squeegee in the reverse direction.

The post-printing treatment involved thermally annealing the AgNW patterns printed on glass in air within a temperature range of 100 to 250 °C to determine the influence of residual solvents and PEO on electrical performance. Fig. 2a illustrates that the resistance of the printed patterns decreased with the increasing annealing temperature for a fixed annealing time of 30 min. The resistance dropped sharply from an initial value of 8.72 Ω to 0.73 Ω at 150 °C and further reduced to 0.71 Ω at 165 °C. Increasing the temperature above 200 °C initiated burning of the AgNWs which negatively impacted the electrical properties. Fig. 2b shows that an annealing temperature of 150 °C and an annealing time of 30 min were sufficient to achieve a minimum resistance. The decrease in resistance of the printed patterns can be attributed to the fusion of the AgNW junctions (Fig. 2c), removal of the solvents, and partial removal of PEO (Fig. 2d).[33] The relatively lower annealing temperature made the post-printing treatment compatible with polymeric substrates like PET, PI and PDMS. PEO is water soluble, however using water washing as a post-printing treatment can be cumbersome and unsuitable on a large scale. Moreover, it can also wash away the AgNWs from the printed pattern impacting its electrical properties.[27,34] Fig. S3a† shows that adopting water-washing as the only post-printing treatment is not enough to achieve the desired electrical conductivity. The resistance after thermal annealing at 150 °C for 30 min (Fig. 2b) was (0.65 ± 0.072) Ω and after seven wash cycles was (6.73 ± 0.135) Ω as shown in Fig. S3a.† Besides, a small amount of residual PEO can provide solvent resistance to the AgNW film. This could be due to the generation of water insoluble substances on possible cross-linking of PEO during the heat treatment process.[27] Cross-linking constraints the PEO chain segments by tying the carbon atoms from different polymer chains together. This way, the original viscous linear segments of the polymer are transformed into an insoluble gel network preventing the polymer chains from escaping into the

Table 1 Viscosity of AgNW Ink B at different shear rates. Each shear rate corresponded to a printing step in the screen-printing process

Screen printing ink	0.1 s^{-1}@20 s	200 s^{-1}@50 s	0.1 s^{-1}@80 s	Recovery@80 s (%)	0.1 s^{-1}@90 s	Recovery@90 s (%)
AgNW–PEO Ink B	134.31	2.56	99.19	73.9	112.54	83.8

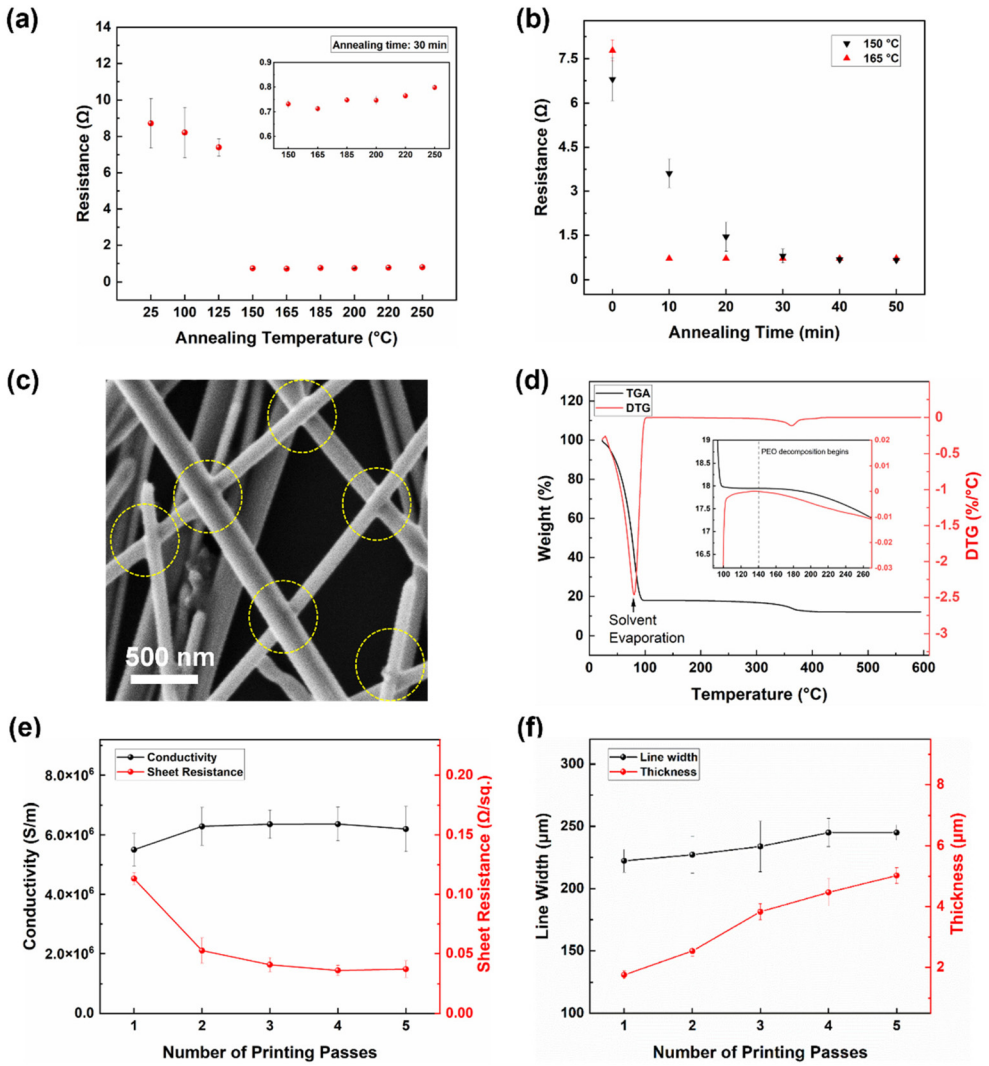

Fig. 2 (a) Influence of the post-printing treatment process. Resistance of screen-printed AgNW patterns as a function of annealing temperature for a fixed time of 30 min. Inset showing the resistance values for the annealing temperature between 150 °C and 250 °C. (b) Variation of the resistance with annealing time for a fixed temperature of 150 °C and 165 °C. (c) High resolution scanning electron microscopy (SEM) image of fused AgNW junctions after post-printing treatment. Scale bar 500 nm. (d) TGA and DTG thermograms of AgNW Ink B. Inset showing TGA and DTG thermograms between 100 and 260 °C. (e) Calculated conductivity and sheet resistance of AgNW lines with increasing printing passes. At least three samples were tested for each line width. (f) Printed line width and thickness of screen printed AgNW lines with increasing rounds of printing passes using a 200 μm designed line width.

solvent solution.[32,35] As expected, the screen printed AgNW patterns showed stable resistance even after immersing them in two different solvents for prolonged time periods (Fig. S3b†).

To further decrease the resistance of the printed patterns and to increase the uniformity, the influence of printing passes was studied. As shown in Fig. 2e, the conductivity of the printed AgNW patterns increased with the second printing pass and remained nearly constant with a further increase of the printing passes. The sheet resistance and conductivity of the printed AgNW patterns after two printing passes and thermal annealing were $0.052 \pm 0.01\ \Omega\ sq^{-1}$ and $(6.29 \pm 0.64) \times 10^6\ S\ m^{-1}$, respectively. The increase in conductivity with the second pass is probably associated with a more uniform printed pattern with fewer printing defects (Fig. S4†). Besides, line width and thickness of the printed patterns increased with the number of passes (Fig. 2f). As increasing the number of printing passes can negatively influence the resolution of the patterns, two printing passes were found to be optimal. The line width of the printed trace increased from 222.4 μm in the first printing pass to 227.2 μm in the second printing pass.

Optical images shown in Fig. 3a represent printed AgNW lines on glass with various line widths of 50, 75, 100, 150 and 200 μm. All the printed lines demonstrated sharp edges and uniform line widths. In this work, a printed line width resolution of 50 μm was achieved. The printed line width and thickness as functions of the designed stencil width are displayed in Fig. 3b. The width of the printed line was slightly larger

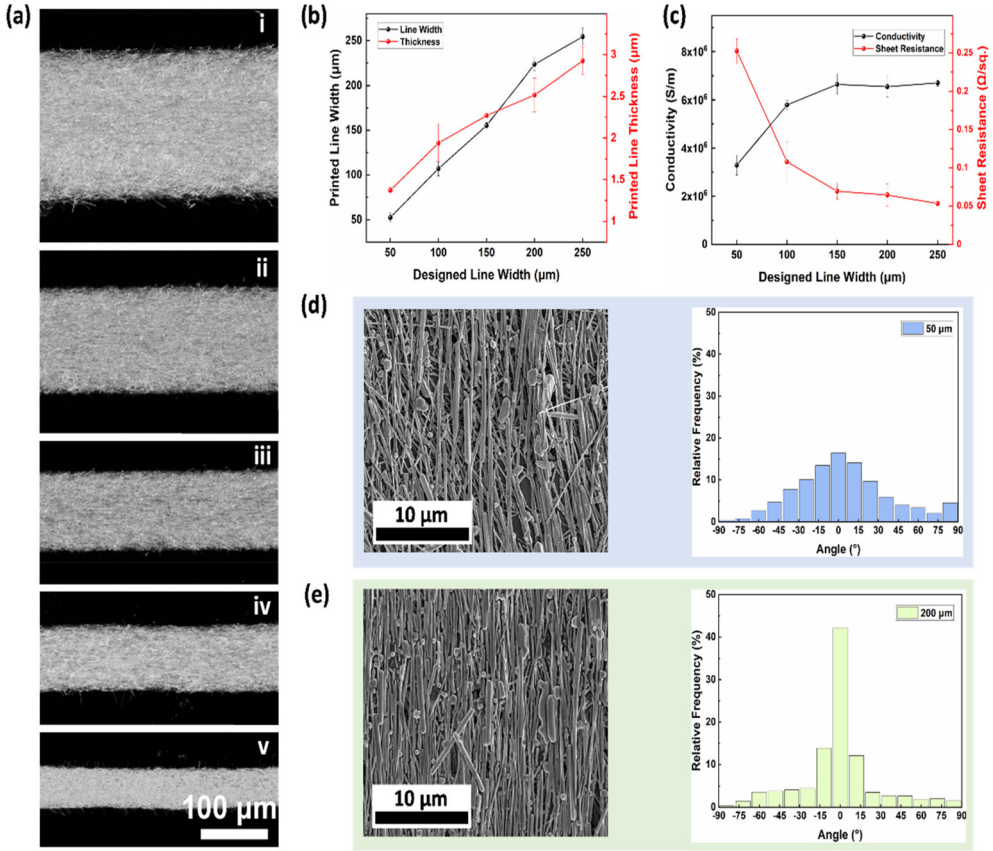

Fig. 3 (a) Optical microscope images of AgNW lines printed on a glass substrate with line widths of (i) 200, (ii) 150, (iii) 100, (iv) 75 and (v) 50 μm. Scale bar 100 μm. (b) Printed line width and thickness of AgNW lines as a functions of the designed line width. (c) Calculated sheet resistance and conductivity of screen printed AgNW lines with various designed line widths. At least three samples were tested for each line width. SEM image of a printed AgNW line and corresponding NW alignment for (d) 50 μm line width and (e) 200 μm line width.

than the designed stencil width, resulting from the combined effect of ink penetration into the gap between the stencil and the substrate and ink spreading after printing.[17] The thickness of the printed lines appeared to increase linearly with line width.

To characterize the electrical properties of the screen-printed patterns, AgNW lines of 6 mm in length with different widths of 50, 100, 150, 200 and 250 μm were printed on a PI tape and thermally annealed. Fig. 3c represents the conductivity and sheet resistance as functions of the designed stencil width. It is seen that the sheet resistance decreases and electrical conductivity increases with the line width. This could be attributed to the differences in AgNW alignment at different line width as shown in Fig. 3d and e. During the printing stroke, the squeegee introduces a shearing force to the AgNWs which can align them in the printing direction.[6] Interestingly, the AgNWs show better alignment along the printing direction for a larger line width. Printing speed is an important parameter in a screen-printing process. Lower printing speed is desired for narrower lines in order to completely transfer the ink onto the substrate (Fig. S5†). In our case, for example, the optimized printing speeds for the line widths of 50 and 200 μm were ~6 and 12 cm s^{-1}, respectively. However, lower printing speed causes lower-degree AgNW alignment. Fig. S6† shows the AgNW alignment for different printed line widths. Better alignment of AgNWs can generally lead to higher conductivity of the printed AgNW patterns. Table 2 compares the resolution, electrical conductivity and post-printing treatment processes between our work and reported screen printing works utilizing different inks. For a low AgNW solid loading (7 wt%) and one-step post printing treatment, lines printed using AgNW Ink B exhibited a better electrical conductivity than those achieved by the Ag particle/flake-based inks.[35]

Besides, the use of a lower sintering temperature (150 °C) in our work makes the process compatible with flexible plastic substrates. The combination of high resolution, high conductivity, and a relatively low-temperature post-printing process, makes our formulated AgNW ink stand out from the previously reported works.

The screen printed AgNW patterns were further characterized to evaluate their flexibility and stretchability, which are a key requirement for wearable electronics.[4] For tensile tests, the AgNW pattern was first printed on a PDMS substrate, and then encapsulated by another layer of PDMS. Fig. 4a and b shows the performance of the AgNW–PDMS conductor under a uniaxial tensile strain. Besides, the AgNW–PDMS conductor showed stable performance even after 450 cycles of tensile stretching and releasing between 0 and 10% strain (Fig. 4c). For testing

Table 2 Comparison of ink composition, line resolution, electrical conductivity, and post-printing treatment in screen printing between various literatures

Screen printing ink	Line resolution (μm)	Electrical conductivity (S m^{-1})	Post-printing treatment	Ref.
Ag NPs, 77 wt%	22	1.81×10^7	(1) Heat: 200 °C, 30 min	17
Ag NPs, 80 wt%	—	2.43×10^7	(1) Heat: 450 °C, 15 min	37
Ag flakes, 43 wt%	50	738×10^2	(1) Heat: 80 °C, 30 min	38
Ag flake, 70 wt%	—	6.67×10^6	(1) Heat at 120 °C for 10 min to remove solvents (2) Heat: 850 °C, 10 min	36
Graphene, 10 mg mL^{-1}		2.8×10^2	(1) Overnight heating at 90 °C or 40 s of microwaving	39
Graphene, 80 mg mL^{-1}	40	1.86×10^5	(1) Heat: 300 °C for 30 min	10
Graphene & carbon black 85 : 15 wt% ratio	90	2.15×10^4	(1) Drying at 100 °C for 8 min. Compressed rolling (2) Drying at 150 °C for 8 min	40
AgNWs, 0.9 wt%	50	5.5×10^6 (for 0.5 mm)	(1) Drying at 80 °C for 10 min to evaporate solvents (2) Immersing AgNW samples in warm water (60 °C) or ethanol for 5 min to remove PVP (3) Illuminating AgNWs by a high-intensity pulsed light with a broad wavelength of 200–1500 nm	41
AgNWs, 1.97 wt%	—	1.9×10^5	(1) Heat at 120 °C for 10 min to remove terpineol (2) Washing in acetone for 2 min to remove ethylene cellulose (3) Washing in ethanol bath for 5 min to remove PVP (4) Laser sintering of AgNWs with Yb:fiber laser	42
AgNWs, 6.6 wt%	50	4.67×10^6	(1) Multiple cycles of heating at 150 °C for 5 min to evaporate the solvent (2) Washing with ethanol and water mixture (1 : 20) for 5 min to remove part of the additives (3) Annealed at 150 °C for 5 min to fuse the AgNW junctions	19
AgNWs, 10 wt%		3.4×10^6	(1) Dry at 110 °C for 10 min	43
AgNWs, 7 wt%	**50**	**6.70×10^6 (for 0.25 mm)**	**(1) Heat: 150 °C for 30 min**	**Our work**

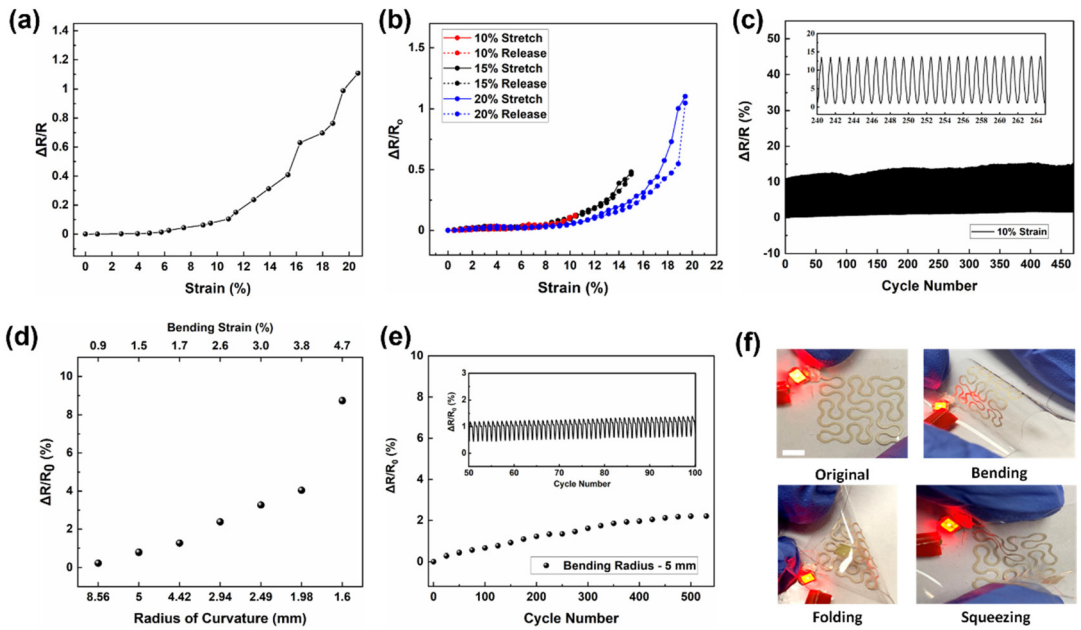

Fig. 4 (a) Resistance change of the screen printed AgNW–PDMS conductor as a function of uniaxial tensile strain (0 to 20.67%). (b) Tensile loading and unloading plot of screen printed AgNW–PDMS composite as a function of tensile strain. (c) Resistance changes under 450 tensile stretching and releasing cycles of 10% strain. (d) Resistance changes as a function of bending curvature radius (8.56–1.6 mm). (e) Resistance changes under 530 bending cycles with 5 mm bending radius and 1.5% bending strain. Inset showing resistance change between 50 and 100 bending cycles. (f) Images of screen printed Peano curve on PDMS under different mechanical deformations of bending, folding, and squeezing. Scale bar: 5 mm.

the bending performance, AgNW patterns were printed on a flexible PET substrate of thickness 0.15 mm. Fig. 4d depicts that the maximum bending strain on the AgNW pattern was 4.68% at the smallest bending curvature radius of 1.6 mm. For the cyclic bending test (Fig. 4e), the resistance of the screen-printed pattern changes only 2% after 530 cycles of bending at

5 mm bending radius and 1.5% bending strain%. Moreover, Fig. 4f shows stable performance (LED light stays turned ON) of a screen printed Peano curve under severe deformation conditions such as bending, folding, and squeezing.

Using the screen-printing process, different AgNW patterns such as lines, curves, and fractal patterns of Peano curve were printed on different substrates such as glass (Fig. 5a–d), PDMS (Fig. 5e–g), textiles (Fig. 5h and i), and PET sheet (Fig. 5j). The optical images reveal that the printed curved lines (Fig. 5k–m) have continuous and smooth boundaries. Compatibility of the current printing process with different substrates along with good electromechanical performance strengthens its adaptability for wearable electronic applications.

To demonstrate the application potential of screen printing, a textile-based flexible heater and a wearable hydration sensor were fabricated. Thermal therapy is widely used to treat osteoarthritis and carpal tunnel syndrome.[44] In the case of osteoar-

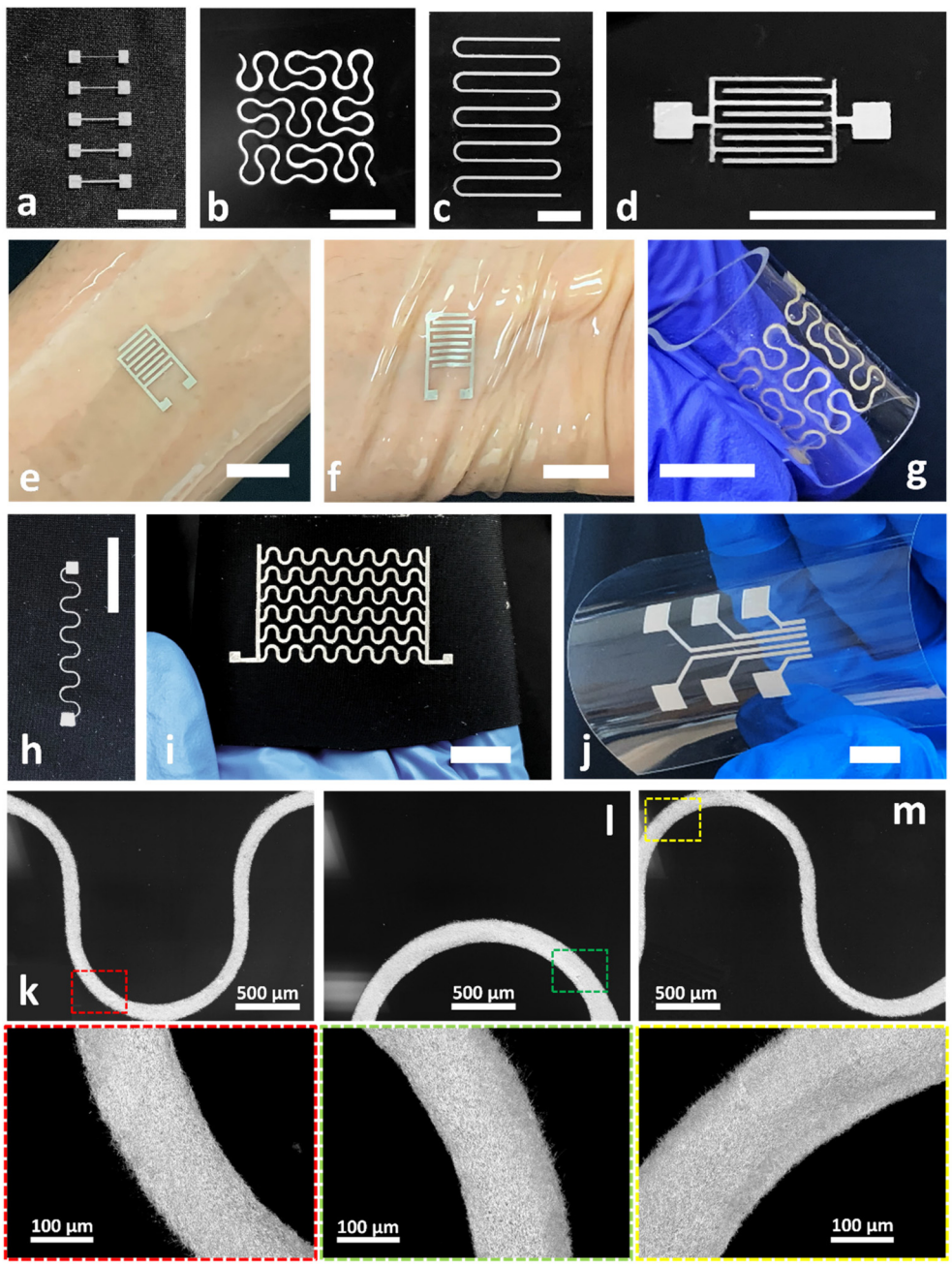

Fig. 5 Demonstration of screen-printing capability. Printed AgNW patterns on glass slide, (a) 50–250 µm lines, (b) Peano curve, (c) curved lines, and (d) interdigitated pattern. Printed AgNW patterns on PDMS, hydration sensor on (e) relaxed wrist, (f) flexed wrist, and (g) Peano curve. Printed AgNW patterns on textile (h) serpentine pattern and (i) serpentine array. (j) AgNW electrode array printed on a PET sheet. Scale bar 10 mm. (k–m) Optical images of printed curved lines with the corresponding insets showing smooth boundaries.

thritis, heat wrap increases tissue temperature which leads to improved blood flow. It also improves muscle extensibility by reducing the stiffness and inflammation of the injured tissue.[45]

It also alleviates pain during rehabilitation in sports related injuries.[46] In this work a textile-based heater was fabricated by directly screen printing the AgNW ink on the textile followed by the post-printing step. The morphology of both the textile and the screen-printed AgNW patterns on the textile was evaluated using confocal microscopy. The maximum height of the profile (R_z) for the textile was found to be 104 μm, showing a high surface roughness. Fig. S7 and S8† show the 3D height maps and thickness profiles of the screen-printed patterns on the textile.

In Fig. 6a, stepwise voltage ranging from 1 to 6 V was applied to the textile-based heater. It can be seen that the

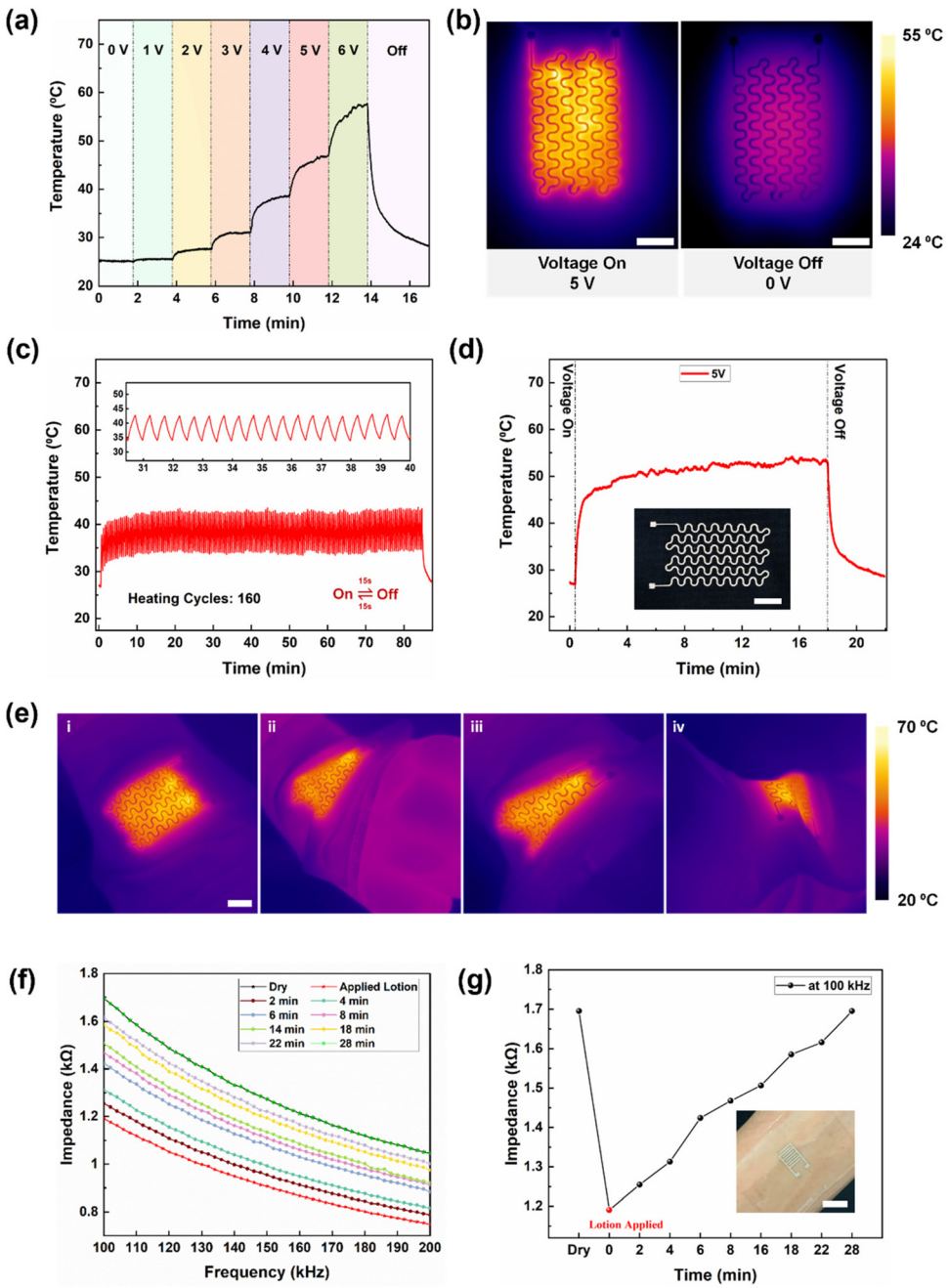

Fig. 6 Screen-printed textile based AgNW heater. (a) Temperature evolution of heater under stepwise voltage from 0 to 6 V. (b) Infrared (IR) thermal image of the textile-based heater at 5 V and 0 V. (c) Temperature evolution of the heater under repeated heating cycle operations (160 cycles). (d) Heater performance for 18 min at 5 V. Inset showing photograph of the textile-based heater. (e) IR images of the heater during (i) relaxed wrist, (ii–iv) various wrist flexing positions. (f) Impedance of the screen-printed wearable hydration sensor before and after applying lotion on the skin. (g) Impedance *versus* time of the hydration sensor at 100 kHz. Inset showing the hydration sensor on the wrist. Scale bar: 10 mm.

temperature of the heater rose with the increasing voltage and at 5 and 6 V, the maximum temperatures were ~46 °C and 57 °C, respectively. Commercial heating pads usually operate in the temperature range of 40 to 60 °C, and therefore further testing on the textile-based heater was done at 5 V.

Fig. 6b shows the infrared (IR) thermal image of the textile-based heater at 5 V. For practical applications, reliability and heating stability of the heater are crucial. Fig. 6c shows 160 heating and cooling cycles on the textile-based heater. In each cycle, a voltage of 5 V was applied to the heater for 15 s and then turned off to naturally cool for 15 s. The temperature ranged between 42 °C and 34 °C. The heater could not return to room temperature (RT) within 15 s due to the relatively slow thermal transport of the textile. Fig. 6d shows the long-term performance of the heater. Fig. 6e depicts the textile heater on the wrist and its stable performance when flexing the wrist. The heater can also withstand different folding deformations as shown in Fig. S9.†

As another application demonstration, an epidermal hydration sensor was screen printed. Skin hydration is a crucial physiological parameter for assessing the status of skin diseases such as eczema, cracking of the stratum corneum, and acne, which can lead to damaged skin and increased transdermal water loss.[47] Although, skin hydration can be obtained through measurements of electrical impedance, thermal conductivity, and spectroscopy, impedance is a direct indicator of hydration due to the high influence of water content on skin permittivity and conductivity.[47] A hydration sensor was fabricated by printing AgNW ink on a glass substrate followed by spin coating liquid PDMS, such that the AgNWs were embedded below the PDMS surface to form a AgNW/PDMS composite.[48,49] To evaluate the performance of the hydration sensor, impedance measurements were performed at different time periods to correlate with the hydration level of the skin. Fig. 6f depicts that impedance dropped sharply after applying the lotion on the skin. At 100 kHz, the impedances before and after applying the lotion were 1.694 kΩ and 1.190 kΩ, respectively (Fig. 6g). As time progressed, the impedance gradually increased and recovered back to its initial level in 28 minutes, similar to previously reported results.[49,50] While the effect of the external ambient conditions on the sensor performance was not characterized in this work, our previous work showed that the hydration sensor produced stable performance in response to skin hydration, regardless of the external environmental conditions of the wearer.[48]

Experimental

Synthesis of AgNWs/PEO

AgNWs were fabricated by a modified polyol process.[51] Firstly, 60 ml of 0.147 M polyvinylpyrrolidone (PVP) (M_v ~ 40 000; Sigma-Aldrich) solution in ethylene glycol (EG) was added to a three-neck round-bottomed flask that was suspended in an oil bath at 151.5 °C. A stir bar was added to the flask and the solution was magnetically stirred at 260 rpm for 1 h. Then, 200 μL of 24 mM $CuCl_2$ ($CuCl_2{\cdot}2H_2O$, 99.999+%; Alfa Aesar) solution in EG was added into the heated solution. After an additional 15 min of heating, 60 ml of 0.094 M $AgNO_3$ (99+%; Sigma-Aldrich) solution in EG was added to the flask. Upon nanowire formation, the solution was cooled to room temperature. Products were washed with acetone first, and then with ethanol. AgNWs were suspended in ethanol for ink preparation.

Preparation of AgNW/PEO ink

Poly(ethylene oxide) powder (PEO, average M_v ~ 1 000 000 purchased from Sigma Aldrich) was first dissolved in a mixed solvent with a 50 : 50 weight ratio of ethanol and deionized water (DI water) to form solutions with different PEO contents (4, 5, 6 and 7 wt%). Then, AgNWs with an average diameter of ~100 nm and an average length of ~25 μm were added into the PEO solutions to make four different screen-printing inks with 7 wt% AgNW solid loading and PEO weight ratio of 4% (Ink A), 5% (Ink B), 6% (Ink C) and 7% (Ink D). The as-prepared inks were magnetically stirred at 1000 rpm for 30 min to ensure an even dispersion.

Screen printing and post-printing treatment of AgNW patterns

Screen printing was performed manually using a ~100 μm thick custom-made stainless-steel stencil from Stencils Unlimited. The stainless-steel stencil was separated from the glass substrate by 2 mm thick PDMS spacers. For printing, AgNW ink was placed on top of the stencil and was manually pushed across the stencil's opening with a rubber squeegee at an angle of ~45° angle with the stencil. The printing speed was manually optimized to ~6 and ~12 cm s^{-1} for narrower (such as 50 μm) and wider (such as 200 μm) line widths, respectively. The printing process was repeated two times for achieving a uniformly printed pattern. Between each printing pass, the sample was baked in an oven at 75 °C for 5 min. The printed AgNW patterns were annealed at 150 °C for 30 min as a post printing treatment step.

The morphologies of the screen printed AgNWs lines were studied by field emission scanning electron microscopy (FESEM) (FEI Quanta 3D FEG) operated at 5 kV. The alignment of the printed AgNW lines was measured by analysing ~1000 AgNWs for each line width in the ImageJ software. The AgNW alignment was distributed from −90° to 90° with 0° indicating the printing direction. An optical microscope (Nikon Eclipse LV150N) was used for obtaining the dimensions of the printed AgNW lines. A 4-probe method was used to measure the resistance of the printed lines using a digital multimeter (34001A, Keysight Technologies). A Keyence VKX1100 confocal laser scanning microscope was used to measure the thickness of the screen-printed patterns and the morphology of the textile. Three samples of each case were tested for calculating the average sheet resistance and conductivity. Rheological behaviour of the formulated AgNW inks was studied using a TA instruments AR-G2 rotational rheometer. A 40 mm diameter parallel plate geometry and a gap height of 850 μm were used for the rheological experiments. All the rheological tests were

performed at the room temperature of 25 °C. A pre-conditioning step of 0.1 s^{-1} shear rate for 15 s was applied before each test. The steady-state flow sweep test was performed by varying the shear rates from 0.1 to 1000 s^{-1}. In the peak hold test, a constant shear rate of 0.1 s^{-1} for 30 s, 200 s^{-1} for 30 s, and 0.1 s^{-1} for 200 s was applied to simulate the screen-printing process. The oscillatory frequency sweep test was performed with a frequency sweep from 0.1 to 100 rad s^{-1}. Storage (G') and loss (G'') moduli were determined through the stress sweep test, performed at an oscillation stress of 1–1000 Pa and a frequency of 100 rad s^{-1}. The stretchability analysis of the screen printed AgNW lines on PDMS was performed using a custom made motorized linear stage and a digital multimeter (Keysight DAQ970A) to monitor the real time resistance change. Before printing, PDMS was treated with oxygen plasma for 1 min to make the surface hydrophilic. AgNW patterns were printed on a flexible PET substrate for evaluating the bending performance. The solvent resistance of the screen printed AgNW pattern was evaluated by submerging the pattern into two different solvents: firstly, 80 : 20 weight ratio of DI water and ethanol and then acetone. Thermal gravimetric analysis (TGA) was performed on a TA Instruments Discovery SDT 650 in air at a rate of 5 °C min^{-1}.

Fabrication of textile-based heater and hydration sensor

AgNW Ink B was screen printed on textile (80% nylon and 20% spandex with a thickness of 0.4 mm) followed by post-printing treatment. For testing, DC power was used to supply current to the heater through the contact pads. An IR camera (FLIR A655sc) was used to record the temperature distribution across the heater.

The hydration sensor was fabricated by screen printing an interdigitated pattern on a glass substrate followed by a post-printing treatment process. Next, liquid PDMS was spin coated at 400 rpm for 30 s on the printed pattern and cured at 75 °C for 3 h. The hydration sensor was peeled off from the glass substrate and then applied on the skin for impedance measurements using a Keysight 4395A impedance analyzer. A sensing frequency of 100–200 kHz was used to evaluate skin hydration levels before and after applying a hydrating lotion on the skin.

Conclusions

In summary, a AgNW based ink containing a relatively low solid loading of 7 wt% AgNWs was developed for screen printing of flexible and stretchable electronics. The formulated AgNW ink, showed a viscosity of 144.45 Pa s at 0.1 s^{-1} shear rate and an appropriate rheological behaviour for screen printing. The use of a biodegradable binder and DI water as a "green solvent" makes the process an eco-friendly printing method. Additionally, the screen-printing process enables printing on a diverse range of substrates including rough textile surfaces which are usually hard to print upon using other printing methods. A single step post-printing treatment with a low thermal annealing temperature of 150 °C for 30 min was developed, leading to a conductivity as high as 6.70×10^6 S m^{-1} even at the low AgNW loading of 7 wt%. Through screen printing, both uniform and sharp-edged lines with a resolution of 50 μm were printed. Complex patterns including interdigitated and Peano fractal patterns were also obtained. A textile-based heater on the wrist was fabricated showing a uniform and stable heating performance under cyclic heating/cooling and various bending deformations. Additionally, an epidermal hydration sensor was printed to measure the impedance of the human skin and correlate the data to the hydration level. The demonstrated results obtained through screen printing of the newly developed AgNW based ink highlighted its potential towards large scale production of wearable printed electronic devices.

Moreover, significant efforts are being made on developing strategies for eco-friendly wearable sensors with the majority of them being either using naturally occurring materials or recyclable materials.[52] For instance, Lei *et al.* developed a biocompatible semiconducting polymer for thin-film transistors utilizing cellulose. The thin-film transistors were fully degraded within 30 days in an acidic environment.[53] Williams *et al.* fabricated an all-carbon based thin-film transistors on paper in which both ink constituents (carbon nanotube and graphene) can be reclaimed and recycled.[54] Future work on recycling of AgNW-based screen-printed electronics can add to the sustainability of the developed process.

Author contributions

D. Shukla and Y. Liu synthesized the silver nanowire used for printing. D. Shukla performed the experiments and analysis. Y. Zhu conceived the research and provided guidance throughout the research. All authors discussed the results and commented on the manuscript.

Conflicts of interest

There are no conflicts to declare.

Acknowledgements

The authors gratefully acknowledge the financial support from the National Science Foundation under award no. 2122841, 2134664, and 1728370 and National Institutes of Health under award no. 1R01HD108473.

Notes and references

1 S. Khan, L. Lorenzelli and R. S. Dahiya, *IEEE Sens. J.*, 2015, **15**, 3164–3185.
2 Y. Goliya, A. Rivadeneyra, J. F. Salmeron, A. Albrecht, J. Mock, M. Haider, J. Russer, B. Cruz, P. Eschlwech,

E. Biebl, M. Becherer and M. R. Bobinger, *Adv. Opt. Mater.*, 2019, **7**, 1–9.
3 Z. Cui, *Printed electronics: materials, technologies and applications*, 2016.
4 Z. Cui, Y. Han, Q. Huang, J. Dong and Y. Zhu, *Nanoscale*, 2018, **10**, 6806–6811.
5 P. Ren, Y. Liu, R. Song, B. O'Connor, J. Dong and Y. Zhu, *ACS Appl. Electron. Mater.*, 2021, **3**, 192–202.
6 H. Lee, B. Seong, J. Kim, Y. Jang and D. Byun, *Small*, 2014, **10**, 3918–3922.
7 N. Mkhize and H. Bhaskaran, *Small Sci.*, 2022, **2**, 2100073.
8 Q. Huang and Y. Zhu, *Sci. Rep.*, 2018, **8**, 1–10.
9 G. Grau, J. Cen, H. Kang, R. Kitsomboonloha, W. J. Scheideler and V. Subramanian, *Flexible Printed Electron.*, 2016, **1**, 2.
10 W. J. Hyun, E. B. Secor, M. C. Hersam, C. D. Frisbie and L. F. Francis, *Adv. Mater.*, 2015, **27**, 109–115.
11 P. F. Moonen, I. Yakimets and J. Huskens, *Adv. Mater.*, 2012, **24**, 5526–5541.
12 P. Zeng, B. Tian, Q. Tian, W. Yao, M. Li, H. Wang, Y. Feng, L. Liu and W. Wu, *Adv. Mater. Technol.*, 2019, **4**, 4–11.
13 Q. Huang and Y. Zhu, *Adv. Mater. Technol.*, 2019, **4**, 1–41.
14 D. Li, X. Liu, X. Chen, W. Y. Lai and W. Huang, *Adv. Mater. Technol.*, 2019, **4**, 1–7.
15 A. S. Pillai, A. Chandran and S. K. Peethambharan, *Appl. Mater. Today*, 2021, **23**, 100987.
16 N. Zavanelli and W. H. Yeo, *ACS Omega*, 2021, **6**, 9344–9351.
17 W. J. Hyun, S. Lim, B. Y. Ahn, J. A. Lewis, C. D. Frisbie and L. F. Francis, *ACS Appl. Mater. Interfaces*, 2015, **7**, 12619–12624.
18 S. Yao, W. Zhou, R. Hinson, P. Dong, S. Wu, J. Ives, X. Hu, H. Huang and Y. Zhu, *Adv. Mater. Technol.*, 2022, **2101637**, 1–11.
19 J. Liang, K. Tong and Q. Pei, *Adv. Mater.*, 2016, **28**, 5986–5996.
20 H. Li, S. Liu, X. Li, Z. S. Wu and J. Liang, *Mater. Chem. Front.*, 2019, **3**, 626–635.
21 Y. Zhang, Y. Zhu, S. Zheng, L. Zhang, X. Shi, J. He, X. Chou and Z. S. Wu, *J. Energy Chem.*, 2021, **63**, 498–513.
22 A. Falco, P. S. Sackenheim, F. J. Romero, M. Becherer, P. Lugli, J. F. Salmerón and A. Rivadeneyra, *Mater. Sci. Eng., B*, 2021, **267**, 115081.
23 L. Liu, Q. Lu, S. Yang, J. Guo, Q. Tian, W. Yao, Z. Guo, V. A. L. Roy and W. Wu, *Adv. Mater. Technol.*, 2018, **3**, 1–9.
24 J. R. Camargo, T. A. Silva, G. A. Rivas and B. C. Janegitz, *Electrochim. Acta*, 2022, **409**, 139968.
25 M. Franco, R. Alves, N. Perinka, C. Tubio, P. Costa and S. Lanceros-Mendéz, *ACS Appl. Electron. Mater.*, 2020, **2**, 2857–2867.
26 R. Faddoul, N. Reverdy-bruas and A. Blayo, *Mater. Sci. Eng., B*, 2012, **177**, 1053–1066.
27 M. Hu, J. Gao, Y. Dong, K. Li, G. Shan, S. Yang and R. K. Y. Li, *Langmuir*, 2012, **28**, 7101–7106.
28 S. Hemmati, D. P. Barkey and N. Gupta, *J. Nanopart. Res.*, 2016, **18**, 1–11.
29 F. Hoeng, A. Denneulin, N. Reverdy-Bruas, G. Krosnicki and J. Bras, *Appl. Surf. Sci.*, 2017, **394**, 160–168.
30 S. Hemmati, D. P. Barkey, N. Gupta and R. Banfield, *ECS J. Solid State Sci. Technol.*, 2015, **4**, P3075–P3079.
31 H. Hong, J. Hu and X. Yan, *ACS Appl. Mater. Interfaces*, 2019, **11**, 27318–27326.
32 M. I. Bahlouli, K. Bekkour, A. Benchabane, Y. Hemar and A. Nemdili, *Appl. Rheol.*, 2013, **23**, 1.
33 W. Zhou, S. Yao, H. Wang, Q. Du, Y. Ma and Y. Zhu, *ACS Nano*, 2020, **14**, 5798–5805.
34 M. Lazár, R. Rado and J. Rychlý, *Adv. Polym. Sci.*, 1990, **95**, 148–197.
35 D. Li, W. Y. Lai, F. Feng and W. Huang, *Adv. Mater. Interfaces*, 2021, **8**, 1–5.
36 W. Songping, *J. Mater. Sci.: Mater. Electron.*, 2007, **18**, 447–452.
37 K. Park, D. Seo and J. Lee, *Colloids Surf., A*, 2008, **313–314**, 351–354.
38 N. Matsuhisa, M. Kaltenbrunner, T. Yokota, H. Jinno, K. Kuribara, T. Sekitani and T. Someya, *Nat. Commun.*, 2015, **6**, 1–11.
39 F. Chen, D. Varghese, S. T. McDermott, I. George, L. Geng and D. H. Adamson, *Sci. Rep.*, 2020, **10**, 1–10.
40 L. Liu, Z. Shen, X. Zhang and H. Ma, *J. Colloid Interface Sci.*, 2021, **582**, 12–21.
41 W. Li, E. Yarali, A. Bakytbekov, T. D. Anthopoulos and A. Shamim, *Nanotechnology*, 2020, **31**, 39.
42 W. Li, S. Yang and A. Shamim, *npj Flexible Electron.*, 2019, **3**(1), 1–8.
43 W. Li, H. Zhang, S. Kagita and A. Shamim, *Adv. Mater. Technol.*, 2021, **6**, 1–8.
44 S. Michlovitz, L. Hun, G. N. Erasala, D. A. Hengehold and K. W. Weingand, *Arch. Phys. Med. Rehabil.*, 2004, **85**, 1409–1419.
45 K. Valdes and T. Marik, *J. Hand Ther.*, 2010, **23**(4), 334–351.
46 S. Yao, J. Yang, F. R. Poblete, X. Hu and Y. Zhu, *ACS Appl. Mater. Interfaces*, 2019, **11**(34), 31028–31037.
47 X. Huang, H. Cheng, K. Chen, Y. Zhang, Y. Zhang, Y. Liu, C. Zhu, S. C. Ouyong, G. W. Kong, C. Yu, Y. Huang and J. A. Rogers, *IEEE Trans. Biomed. Eng.*, 2013, **60**(10), 2848–2857.
48 F. Xu and Y. Zhu, *Adv. Mater.*, 2012, **24**(37), 5117–5122.
49 S. Yao, A. Myers, A. Malhotra, F. Lin, A. Bozkurt, J. F. Muth and Y. Zhu, *Adv. Healthcare Mater.*, 2017, **6**(6), 1–8.
50 Y. Liu, H. Wang and Y. Zhu, *Adv. Electron. Mater.*, 2021, **7**(9), 1–11.
51 K. E. Korte, S. E. Skrabalak and Y. Xia, *J. Mater. Chem.*, 2008, **18**(4), 437–441.
52 Y. Liu, S. Shang, S. Mo, P. Wang and H. Wang, *Int. J. Precis. Eng. Manuf. – Green Technol.*, 2021, **8**, 1323–1346.
53 T. Lei, M. Guan, J. Liu, H. C. Lin, R. Pfattner, L. Shaw, A. F. McGuire, T. C. Huang, L. Shao, K. T. Cheng, J. B. H. Tok and Z. Bao, *Proc. Natl. Acad. Sci. U. S. A.*, 2017, **114**, 5107–5112.
54 N. X. Williams, G. Bullard, N. Brooke, M. J. Therien and A. D. Franklin, *Nat. Electron.*, 2021, **4**, 261–268.

